Thermal quenching of photoluminescence in ZnO/ZnMgO multiple quantum wells following oxygen implantation and rapid thermal annealing

Xiaoming Wen [a,b,c,*], J.A. Davis [c], L.V. Dao [c], P. Hannaford [c], V.A. Coleman [d], H.H. Tan [d], C. Jagadish [d], K. Koike [e], S. Sasa [e], M. Inoue [e], M. Yano [e]

[a] Department of Physics, Yunnan University, Kunming 650091, PR China
[b] School of Chemistry, University of Melbourne, Victoria 3010, Australia
[c] Centre for Atom Optics and Ultrafast Spectroscopy, Swinburne University of Technology, Victoria 3122, Australia
[d] Department of Electronic Materials Engineering, Research School of Physical Sciences and Engineering, The Australian National University, Canberra ACT 0200, Australia
[e] Nanomaterials Microdevices Research Center, Osaka Institute of Technology, Asahi-ku Ohmiya, Osaka 535-8585, Japan

ARTICLE INFO

ABSTRACT

The temperature-dependent photoluminescence in oxygen-implanted and rapid thermally annealed ZnO/ZnMgO multiple quantum wells is investigated. A difference in the thermal quenching of the photoluminescence is found between the implanted and unimplanted quantum wells. Oxygen implantation and subsequent rapid thermal annealing results in the diffusion of magnesium atoms into quantum wells and thus, leads to an increased fluctuation in the potential of the quantum wells and the observation of a large thermal activation energy. However, a high dose of implantation results in large defect clusters and thus an additional nonradiative channel, which leads to a flat potential fluctuation and a small thermal activation energy.

© 2008 Elsevier B.V. All rights reserved.

1. Introduction

Zinc oxide has recently attracted considerable interest due to its important potential application in the fabrication of short wavelength optoelectronic devices and in high-temperature/high-power electronics based on its large fundamental band gap of 3.3 eV and large exciton binding energy of 60 meV at room temperature [1]. Being a direct band gap light emitter ZnO alloyed with MgO or CdO can be tuned from the ultraviolet to the red [2] and thus has great prospects in optoelectronics applications. Moreover, excitons in ZnO-based quantum well (QW) hetero-structures exhibit high stability compared to bulk semiconductors or III–V QWs due to the enhancement of the binding energy and the reduction of the exciton–phonon coupling [3,4] caused by quantum confinement.

Band gap engineering can effectively tune the emission wavelength for further ZnO applications, e.g., alloying ZnO with MgO [5] can generate blue-shifts in the emission wavelengths by changing the Mg composition [6,7] or by inducing thermal intermixing in the ZnO/ZnMgO QWs by annealing [8–11]. Ion implantation-induced intermixing has two main advantages. One is the number of defects introduced by ion irradiation can be precisely controlled, thus controlling the amount of wavelength shifting; and the other is no further processing and regrowth are required. Point defects induced by ion irradiation usually act as nonradiative centres, which result in a substantial reduction in the photoluminescence (PL) efficiency. Therefore, subsequent rapid thermal annealing (RTA) is performed to remove the remaining defects to recover the optical properties and to initiate the interdiffusion process. In addition to band gap tuning, ion implantation and subsequent rapid annealing also induces other effects, such as suppression of the internal electric field [12] and changes in the thermal quenching of the PL [13].

Extensive investigations have been performed on ion implantation in ZnO bulk and various nanostructures [14–17]. It has been shown that ZnO exhibits an extremely high dynamic annealing and remains crystalline even after bombardment by rather high doses of ions [1,17]. Such efficient dynamic annealing of ion-beam-generated defects results in an effective recovery of the optical quality of ZnO QWs. At the same time ion implantation followed by RTA also changes the thermal quenching rate of the

PL. However, ion implantation and the effective annealing result in a complicated mechanism in the accumulation of damage and the recovery behaviour in ZnO QWs. The detailed physical mechanism for the variation of the thermal activation energy in ZnO/ZnMgO QWs is not well understood. In this investigation the thermal quenching effect of PL induced by implantation and annealing is studied in ZnO/ZnMgO QWs of different widths.

2. Experiment

The samples used in this experiment are single crystal stack of 19 $ZnO/Zn_{0.7}Mg_{0.3}O$ multiple QWs (MQWs) grown on a-plane sapphire by molecular beam epitaxy, including three groups with the same barrier thickness of 5.5 nm and different width of the QWs, 2, 3 and 4 nm, respectively. After growth, the samples were irradiated with 80 keV O^- ions in the dose range 5×10^{14}–1×10^{16} cm^{-2} at room temperature, using a 1.7 MV tandem accelerator (NEC, 5SDH-4), followed by RTA at 800 °C in an argon ambient for 60 s. The ion implantation and subsequent RTA leads to inter-diffusion of the Zn and Mg atoms in the barrier and the well, thus allowing fine control of the band gap of the QW. A piece of Si was used to mask a part of the sample during implantation to be used as a reference.

The excitation laser used in the PL experiment has a wavelength of 266 nm from a Ti:sapphire regenerative amplifier, pulse duration 100 fs and repetition rate 1 kHz. The detector is a UV–visible response photomultiplier tube at the output slit of a 0.25 m monochromator. The QW sample was mounted in a closed-cycle helium cryostat with a variable temperature ranging from 20 to 300 K.

3. Experimental results and discussion

The near-band edge PL spectra were observed for the implanted and reference samples at 20 K. For each width of the QWs an increased blue shift of the PL was observed with increasing implantation dose, which is consistent with the cathodoluminescence results of Coleman et al. [11], as shown in Fig. 1 for 2 nm QWs samples. For each width of the QWs a slightly increased PL intensity was observed in the implanted samples with doses from 5×10^{14} to 5×10^{15} ions/cm^2, which suggests that
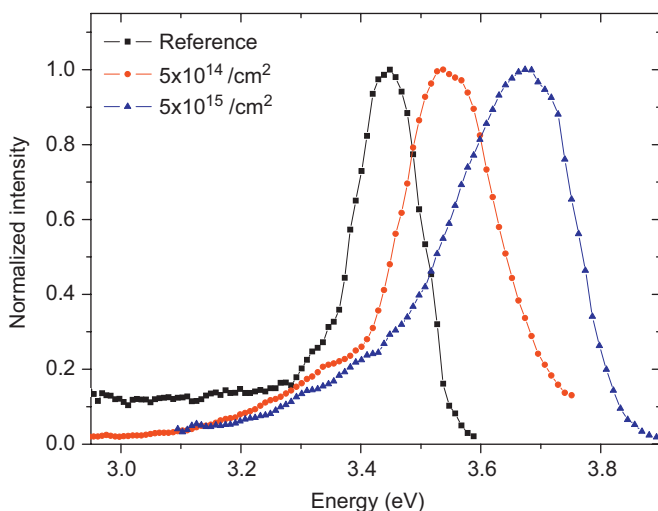
Fig. 1. Photoluminescence of 2 nm width ZnO/ZnMgO multiple quantum wells: reference and implanted samples. An increased blue shift is observed with increasing implantation dose.
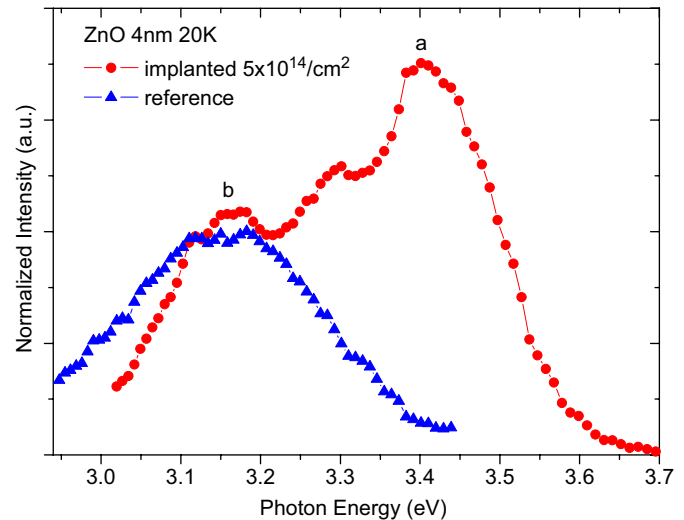
Fig. 2. Photoluminescence spectra at 20 K for implanted and reference ZnO/ZnMgO multiple quantum wells of 4 nm width. Peaks (a) and (b) correspond to the quantum wells that receive full implantation and virtually no implantation, respectively.

the defects created in the implantation process were well recovered due to very effective dynamic annealing. However, for an even higher dose, 1×10^{16} ions/cm^2, the intensity of the PL decreases significantly for each width of the QWs because the high irradiation dose leads to extensive lattice damage and forms point defect complexes associated with a zinc vacancy ($V_{Zn}-X$) that act as nonradiative centres [18].

For 3 and 4 nm width of QWs a similar blue shift is observed in PL spectrum. However, a broad shoulder in the low energy side is observed, as shown in Fig. 2 for the samples of 4 nm width with 5×10^{14} ions/cm^2 (circles) implantation and the reference (triangles). The PL band for ZnO/ZnMgO MQWs has been studied and attributed mainly to transitions involving excitons [19]. For the small width of QWs the PL contribution from phonon replica is significantly reduced due to the strong quantum confinement effect [20]. In contrast in the large width of QWs the enhanced quantum confinement Stark effect [11] and weak quantum confinement totally result in a red shift. And the broad PL spectrum of the reference is most likely due to various transitions overlapping, including emission from excitons and phonon replica.

In the ion implantation and subsequent RTA processes, the defects created by ion implantation drive the energy shift by interdiffusion of Zn atoms from the ZnO wells into the barrier layers and Mg atoms from the barrier layers into the ZnO wells. Upon annealing, these defects become mobile and initiate the interdiffusion process. However, ion irradiation does not create uniform point defects in all QWs and thus there is a different amount of intermixing in the thick QWs. Fig. 3 shows the calculated displacement density expected during oxygen implantation as a function of depth, based on TRIM code calculations [21], and the location of the MQW sample with respect to the displacement profile [11]. According to the TRIM code calculations, the intermixing effect induced by implantation occurs mainly in the front 80–100 nm of the QW surface region. For 4 nm width of QWs, the total thickness of the active region is $19 \times (4+5.5) = 180$ nm. This means that only the top 7–10 QWs receive the full implantation dose and the other half of the QWs experience low dose implantation or virtually no implantation.

Clearly separated exciton PL peaks are observed for the implanted samples of 3 and 4 nm due to the blue shift depending on the displacement density induced by the oxygen implantation.
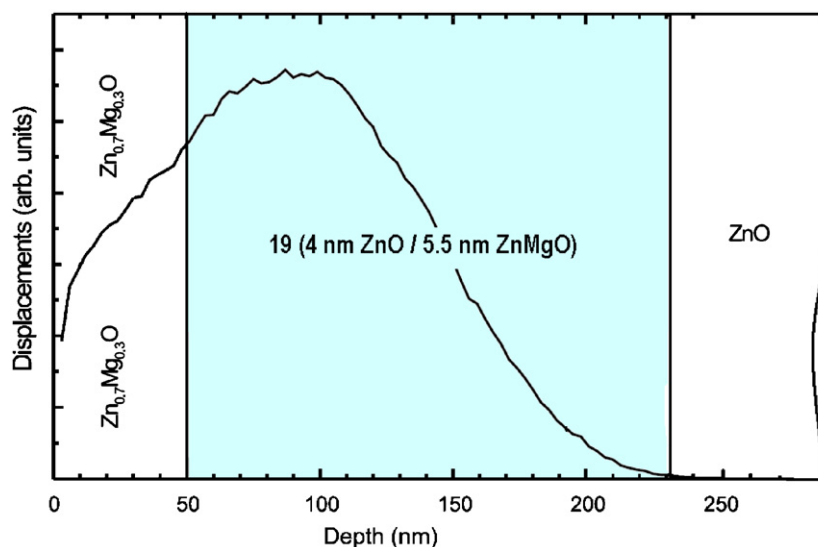
Fig. 3. Displacement density as a function of depth in the 80 keV oxygen irradiation as calculated from TRIM in a 4 nm width ZnO/ZnMgO multiple quantum well sample. Only the front part of the quantum wells receives the full implantation dose.
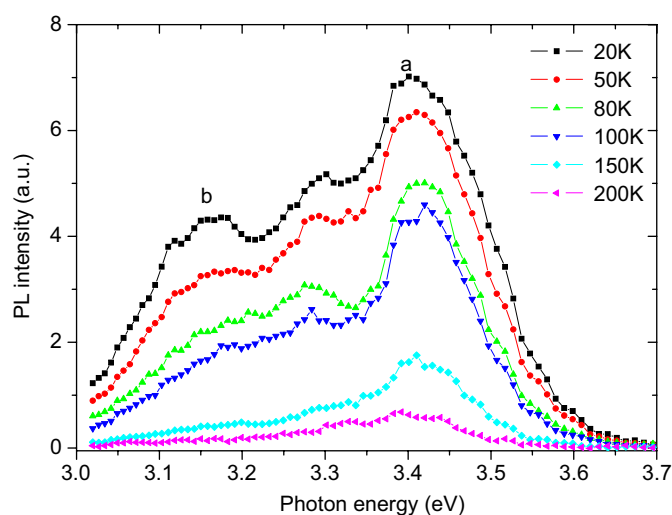
Fig. 4. Temperature dependence of the PL intensity in 4 nm width implanted ZnO/ZnMgO MQWs with a dose of $5 \times 10^{14}\,\mathrm{cm^{-2}}$.

Fig. 5. Arrhenius plot of the PL intensity of peaks a and b for the 4 nm width of QWs. The activation energies at the peaks of a and b are deduced from the fits. A similar value of 23 meV is deduced from the reference sample of 4 nm.

A peak with significant blue shift (a) is attributed to exciton transitions of the QWs that received the full implantation dose. This peak is significantly narrower than the emission band of the reference. Another PL peak (b) is observed at around 3.15 eV, and it is attributed mainly to QWs with virtually no implantation. Similarly evident broadening PL band in implanted QWs of 2 nm (Fig. 1) results from inhomogeneous implantation in the QWs.

With increasing temperature the intensity of the PL decreases for each sample. However, different PL quenching rates are observed in the implanted and reference samples. To compare the temperature quenching variation induced by implantation and RTA, an activation energy is introduced to describe the PL intensity quenching process [21]

$$I = I_0/[1 + \alpha \exp(-E_a/k_B T)] \tag{1}$$

where $\alpha = \tau_R/\tau_0$, τ_R and τ_{NR} are radiative and nonradiative lifetimes, respectively, with $\tau_{NR} = \tau_0 \exp(E_a/k_B T)$, E_a is the activation energy and k_B is Boltzmann's constant.

We measured temperature dependence of the PL. Fig. 4 shows the PL spectra of 4 nm width QWs implanted with a dose of

5×10^{14} ions/cm² and the corresponding Arrhenius plots is shown in Fig. 5. Activation energies of 35 and 24 meV are deduced by fitting the Arrhenius plots using Eq. (1) for peaks a and b, corresponding to full implanted and virtually no implanted QWs, respectively. A closed activation energy of 23 meV is deduced for the reference of 4 nm QWs. Similarly, thermal activation energies for the 2, 3 and 4 nm width of QWs were deduced and shown in Fig. 6. Theoretical modelling of the implantation-induced interdiffusion was performed by assuming that Fick's second law of diffusion applies and thus the diffusion lengths are independent of the well width [11]. The diffusion lengths of Mg into the QWs were calculated and are shown in Fig. 6 (triangles).

Each reference sample shows a low activation energy and the reference of 4 nm gives a slightly higher activation energy than those of 2 and 3 nm. This possibly is due to a small fraction of the PL from phonon replica although exciton emission is dominant. At low dose of implantation each implanted sample shows a
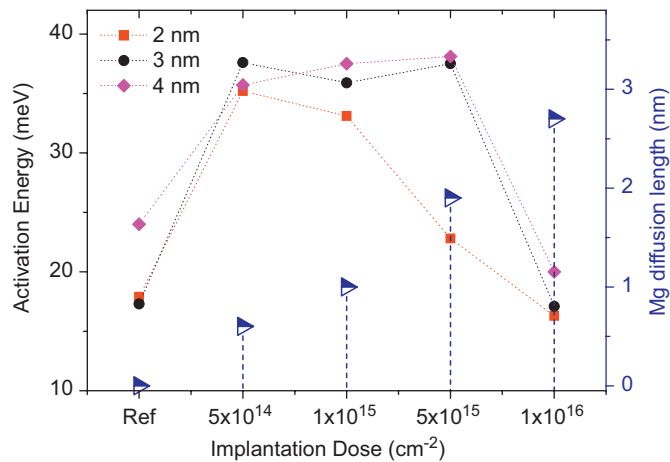
Fig. 6. Thermal activation energy deduced from the temperature dependence of photoluminescence in 2, 3 and 4 nm width QWs for implantation with different doses and the references. The corresponding Mg diffusion lengths into the QWs obtained from the theoretical modelling are also shown (triangles).

significantly increased activation energy. With further increasing implantation dose, however the activation energy for 2 nm width QWs decreases at the irradiation dose of 5×10^{15} cm^{-2}, corresponding to Mg diffusion length of 1.9 nm. At the even larger dose of 1×10^{16} cm^{-2}, which corresponds to Mg diffusion length of 2.7 nm, the activation energy for each width decreases significantly, roughly equal to that of the references.

The temperature quenching of the PL in a QW system is generally explained by thermal emission of carriers out of a confining potential with an activation energy correlated with the depth of the confining potential. Thermal quenching of the PL is not due to the thermal activation of electrons or holes from ZnO QWs into the ZnMgO barriers because the observed activation energy is much smaller than the band offsets as well as the band gap difference between the QWs and the barriers. The activation energy is also significantly smaller than the exciton binding energy that is >60 meV due to quantum confinement enhancement [22]. Thus, the mechanism of thermal quenching of the excitons is not possible. In the case of oxygen implantation, a myriad of defects can be generated, such as zinc vacancies and interstitials, oxygen vacancies and interstitials, and anti-sites, although dynamic annealing of the point defects generated by ion implantation in ZnO is extremely efficient [16]. Supposed that the thermal quenching of the PL is due to the electrons or holes in the QWs captured into a fixed defect state then oxygen ion implantation and subsequent RTA will lead to a decreased, rather than an increased, activation energy because implantation and RTA result in an increased band gap of the QWs. The mechanism for the temperature quenching of the PL intensity most likely is thermionic emission of the excitons out of the potential minima at the interface between the QWs and the barriers [11]. During implantation and RTA Mg atoms will partially replace Zn atoms and form ZnMgO alloy, thereby forming a deeper potential fluctuation and a higher thermal activation energy.

For the low implantation doses, 5×10^{14}–1×10^{15} cm^{-2}, corresponding to the small diffusion lengths 0.6 and 1.0 nm, Mg atoms diffuse into the wells where they partially form ZnMgO alloy in the ZnO lattice. A large fluctuation of the potential occurs and thus a large activation energy was observed, possibly due to the potential difference between ZnO and ZnMgO.

At high dose of implantation the diffusion length increases, which means a complete intermixing for 2 nm width QWs

because of the Mg diffusion length, 1.9 nm, is comparable with the width of the QWs. This will significantly increase the concentration of Mg atoms in the QW and thus the concentration of ZnMgO alloy in the ZnO lattice, which will lead to a flat potential fluctuation and thus decreased the activation energy. Another factor may also affect activation energy. At the very high irradiation dose, 1×10^{16} cm^{-2}, extensive lattice damage occurs and large defect clusters form although extremely high annealing dynamics in ZnO. These point defect complexes associated with zinc vacancy (V_{Zn}−X) probably act as nonradiative centres where excitons in the QWs are nonradiatively trapped. Therefore, the intensity of the PL decreases significantly for each width of QWs and corresponding activation energy decreases. However, further work is required to better understand the mechanism of ion implantation-induced defect complexes and how they act as nonradiative centre in ZnO QWs.

4. Conclusion

We have investigated thermal quenching of the PL in oxygen-implanted and rapid thermally annealed ZnO/ZnMgO MQWs. A difference in the thermal quenching of PL was observed between the implanted and unimplanted QWs. Oxygen implantation and RTA resulted in the diffusion of magnesium atoms into the QWs, which leads to an increased fluctuation in the potential and thus a large thermal activation energy. Large defect clusters induced by high dose of implantation and the large diffusion length of Mg result in a flat potential fluctuation and thus a small thermal activation energy.

Acknowledgements

References

[1] U. Ozgur, Y.I. Alivov, C. Liu, A. Teke, M.A. Reshchikov, S. Dogan, V. Avrutin, S.J. Cho, H. Morkoc, J. Appl. Phys. 98 (2005) 041301.
[2] T. Makino, Y. Segawa, M. Kawasaki, H. Koinuma, Semicond. Sci. Technol. 20 (2005) S78.
[3] H.D. Sun, Y. Segawa, M. Kawasaki, A. Ohtomo, K. Tamura, H. Koinuma, J. Appl. Phys. 91 (2002) 6457.
[4] H.D. Sun, T. Makino, Y. Segawa, M. Kawasaki, A. Ohtomo, K. Tamura, H. Koinuma, J. Appl. Phys. 91 (2002) 1993.
[5] T. Gruber, C. Kirchner, R. Kling, F. Reuss, A. Waag, Appl. Phys. Lett. 84 (2004) 5359.
[6] A. Ohtomo, M. Kawasaki, I. Ohkubo, H. Koinuma, T. Yasuda, Y. Segawa, Appl. Phys. Lett. 75 (1999) 980.
[7] K. Koike, K. Hama, I. Nakashima, S. Sasa, M. Inoue, M. Yano, Jpn. J. Appl. Phys. 44 (2005) 3822.
[8] J. Kennedy, A. Markwitz, Z. Li, W. Gao, C. Kendrick, S.M. Durbin, R. Reeves, Curr. Appl. Phys. 6 (2006) 495.
[9] H.M. Zhong, X.S. Chen, J.B. Wang, C.S. Xia, S.W. Wang, Z.F. Li, W.L. Xu, W. Lu, Acta Phys. Sin. 55 (2006) 2073.
[10] I. Sakaguchi, Y. Sato, H. Ryoken, S. Hishita, N. Ohashi, H. Haneda, Jpn. J. Appl. Phys. 44 (2005) L1289.
[11] V.A. Coleman, M. Buda, H.H. Tan, C. Jagadish, M.R. Phillips, K. Koike, S. Sasa, M. Inoue, M. Yano, Semicond. Sci. Technol. 21 (2006) L25.
[12] J.A. Davis, L.V. Dao, X.M. Wen, C. Ticknor, P. Hannaford, V.A. Coleman, H.H. Tan, C. Jagadish, K. Koike, S. Sasa, M. Inoue, M. Yano, Nanotechnology 19 (2008) 055205.
[13] X.M. Wen, J.A. Davis, L. Van Dao, P. Hannaford, V.A. Coleman, H.H. Tan, C. Jagadish, K. Koike, S. Sasa, M. Inoue, M. Yano, Appl. Phys. Lett. 90 (2007) 221914.
[14] T. Koida, A. Uedono, A. Tsukazaki, T. Sota, M. Kawasaki, S.F. Chichibu, Phys. Status Solidi A 201 (2004) 2841.
[15] Z.Q. Chen, T. Sekiguchi, X.L. Yuan, M. Maekawa, A. Kawasuso, J. Phys. Condens. Matter 16 (2004) S293.

[16] K.P. Vijayakumar, P.M.R. Kumar, C.S. Kartha, K.C. Wilson, F. Singh, K.G.M. Nair, Y. Kashiwaba, Phys. Status Solidi A 203 (2006) 860.
[17] S.O. Kucheyev, J.S. Williams, C. Jagadish, J. Zou, C. Evans, A.J. Nelson, A.V. Hamza, Phys. Rev. B 67 (2003) 094115.
[18] S.F. Chichibu, T. Onuma, M. Kubota, A. Uedono, T. Sota, A. Tsukazaki, A. Ohtomo, M. Kawasaki, J. Appl. Phys. 99 (2006) 093505.
[19] T. Makino, Y. Segawa, M. Kawasaki, J. Appl. Phys. 97 (2005) 106111.
[20] C. Morhain, T. Bretagnon, P. Lefebvre, X. Tang, P. Valvin, T. Guillet, B. Gil, T. Taliercio, M. Teisseire-Doninelli, B. Vinter, C. Deparis, Phys. Rev. B 72 (2005) 241305.
[21] T. Makino, K. Tamura, C.H. Chia, Y. Segawa, M. Kawasaki, A. Ohtomo, H. Koinuma, J. Appl. Phys. 93 (2003) 5929.
[22] Y.H. Cho, G.H. Gainer, A.J. Fischer, J.J. Song, S. Keller, U.K. Mishra, S.P. DenBaars, Appl. Phys. Lett. 73 (1998) 1370.